Supporting Information for

Luminescent Optical Detection of Volatile Electron Deficient Compounds by Conjugated Polymer Nanofibers

Aidan Wade[§], Pierre Lovera,[†] Deirdre O'Carroll,[‡] Hugh Doyle,[†,] and Gareth Redmond[§,]**

* To whom correspondence should be sent. Email: hugh.doyle@tyndall.ie and gareth.redmond@ucd.ie.

RECEIVED DATE

[§] School of Chemistry and Chemical Biology, University College Dublin, Belfield, Dublin 4, Ireland

[†] Tyndall National Institute, Lee Maltings, Cork, Ireland.

[‡] Department of Materials Science and Engineering, Rutgers, The State University of NJ, 607 Taylor Road, Piscataway, NJ 08854, USA.

Materials

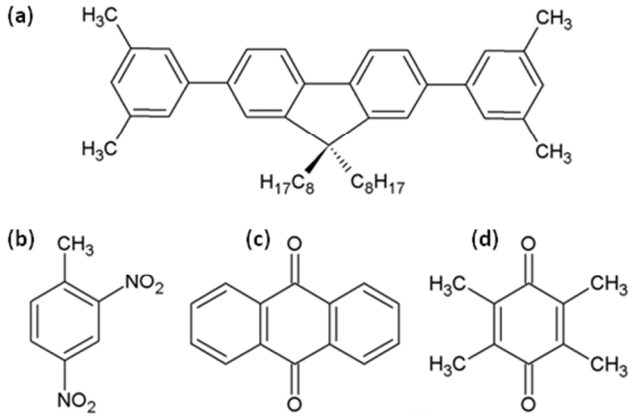

Scheme SI.1 Molecular structures of (a) PFO, (b) 2,4-DNT, (c) AQ, and (d) DQ.

Sample Substrates

Glass cover slips, 11 mm × 22 mm (6663-Q10) and 20 mm × 20 mm in size, respectively, were obtained from Thomas Scientific, Ltd. and Menzel GmbH & Co. K.G., respectively, and were employed for various tasks. These substrates were "acid cleaned" by immersion in 1:1 HCl: methanol (30 min), rinsing in de-ionized water (× 2), immersion in H_2SO_4 (30 min), rinsing in deionized water (× 3) and finally, drying under nitrogen (N_2) gas flow.

PFO Samples

To make PFO thin films, PFO solutions were prepared by dissolving 0.5 mg of PFO in 1 mL of $CHCl_3$, and stirring at 60 ^oC for 1 hr. All polymer solutions were subsequently filtered using 0.2 μm pore size Acrodisk® PTFE syringe filters (Pall Corp.) to remove any non-dissolved material. Polymer thin films were then prepared by spin-coating a droplet of the PFO solution onto a cleaned glass cover slip at 6000 rpm for 60 s using a spin coater (KW-4B, CHEMAT Technology, Inc.). To synthesize PFO nanofibers, a concentrated solution of PFO (60 mg/mL),

was prepared by dissolving the polymer in anhydrous THF in a sealed amber glass vial, while heating to 60 ^{o}C, and stirring vigorously for 30 min. The resulting solution was allowed cool to room temperature. It appeared clear and slightly viscous upon visual inspection. Alumina membranes were sonicated in methanol and air-dried prior to use. An alumina membrane was placed onto a glass slide and a 50 μL drop of polymer solution was deposited on top of the membrane. A glass cover slip was placed on top of the drop on the membrane, facilitating penetration of the solution into the template pores. A weight of *ca.* 2.5 kg was applied overnight in order to maximize pore wetting by the solution and to facilitate formation of nanofibres. Following this, any excess material that had not penetrated the alumina template pores was removed from the surface of the template by manually scraping with a razor blade. The template, with embedded nanofibers, was soaked in aqueous NaOH (3 M) for 12 hr in order to dissolve the alumina host. Following nanofiber release, the NaOH solution was removed using a pipette and the nanofiber residue was gently washed three times with de-ionized water and once with acetone before finally dispersing the fibers in decane (with sonication for *ca.* 2 s). The final nanofiber dispersions were pale yellow in color under ambient room conditions. All template synthesis steps, from weighing to dissolution of the PFO material, were carried out in ambient atmosphere conditions. Random arrays of nanofibers were prepared by depositing 5 μL droplets of nanofibers, suspended in decane, onto acid cleaned glass cover slips followed by drying overnight in air, in the dark, at room temperature. These samples were stored in a sealed box prior to use.

Sample Imaging

Luminescence microscopy images of nanofibers were acquired using a calibrated upright epi-fluorescence microscope (BX51, Olympus Corp.) equipped with a 100 W halogen lamp and a thermoelectrically cooled color CCD camera (Fast1394 QICAM, QImaging, Ltd.). For imaging of PFO nanofibres, the halogen lamp was used in conjunction with a filter set that enabled sample excitation at between 370 nm and 412 nm and collection of resulting luminescence above 415 nm (Semrock, Inc.). The images were captured and analyzed using QCapture Pro™ software (QImaging, Ltd.).

Optical Measurements

UV-vis absorption spectra were acquired using a double-beam spectrophotometer (V-650, Jasco, Inc.) equipped with an optional 60 mm integrating sphere (ISV-722, Jasco, Inc.). To measure an absorption spectrum of a polymer thin film or a random nanofiber array on a glass cover slip, the slip was placed into the spectrometer at 90^{o} to the incident beam; a blank cover slip was used for background subtraction. Photoluminescence (PL) spectra were recorded (393 nm excitation) using two luminescence spectrometers: One equipped with a pulsed Xe short arc discharge lamp and Czerny-Turner monochromators (QuantaMaster™ 40, Photon Technology International, Inc.) and another routine system (LS 50B, Perkin Elmer, Ltd.). Thin film and nanofiber samples (on 11 mm × 22 mm cover slips) were mounted at 45^{o} to the incident beam using a home-built coverslip holder in a 10 × 10 mm quartz cuvette (101-QS, Hellma® GmbH & Co. K.G.) that was placed into the temperature controlled cuvette holder (TLC 50™, Quantum Northwest, Inc.) of the QuantaMaster™ 40 system.

Emission Quenching Studies on Single Nanofibers

Single nanofiber emission measurements were carried out using a scanning confocal PL microscope (MicroTime 200, PicoQuant GmbH) equipped with a XY piezoelectric scanning stage (P-733-2CL, Physik Instrumente GmbH). System operation was controlled by a dedicated software package (MicroTime 200 Version 4.0 software, PicoQuant GmbH). The output of a 402 nm pulsed picosecond laser diode (pulse width of 70 ps, repetition rate of 40 MHz, LDH-P-C-400, PicoQuant GmbH) was spectrally filtered using a 405 nm band pass filter (Z405/10X, Chroma Technology Corp.) and then converted to circularly polarized light using a broadband quarter waveplate (AQWP05M-630, Thorlabs Inc.). The collimated laser beam was then directed into the entrance port of an inverted microscope (IX 71, Olympus Corp.) using a dichroic mirror (Z405rdc, Chroma Technology Corp.). A 100× oil immersion objective (NA of 1.4, UPlan SAPO, Olympus Corp.) was used both for focusing the excitation light onto the sample (a random nanofiber array deposited onto a cleaned glass cover slip at sub-monolayer coverage) on the piezoelectric scanning stage and for collecting the resulting photoluminescence. The luminescence was passed back through the dichroic mirror, spatially filtered by focusing onto a 50 μm diameter pinhole to reject out-of-focus signals, re-collimated, and directed onto an avalanche photodiode (SPCM-AQR-14, Perkin-Elmer Inc.). Backscattered excitation light was blocked using a 430 nm long pass filter (HQ430LP, Chroma Technology Corp.) placed in the collection path.

Scanning confocal emission intensity images of single nanofibers were recorded by raster scanning the sample through the laser focus spot and recording the resulting luminescence at the avalanche photodiode. All emission images were recorded with a pixel integration time of 2 ms and an incident excitation power < 0.1 nW/cm^2 to prevent problems associated with

photobleaching. Emission intensity time traces of single nanofibers were carried out by positioning the fiber at the focus spot of the excitation laser beam and recording the emission intensity measured at the avalanche photodiode versus time. Single nanofiber PL spectra were recorded by directing the emitted light onto the entrance slit of a monochromator equipped with a 300 g/mm grating (SP2356, Acton Research Corp.) and a thermoelectrically cooled, back illuminated CCD (Spec10:100B, Princeton Instruments Inc.). PL spectra were typically recorded with an input slit width of 500 μm and an integration time of 30 s.

Emission quenching in single PFO nanofibers was monitored by placing a solid sample of 2,4-DNT material onto a metal mesh lying 5 mm above a nanofiber array; see Scheme SI.2. In a typical experiment, a scanning confocal emission intensity image and a spatially resolved PL spectrum were recorded for an individual nanofiber at room temperature under ambient conditions. Following this, the emission intensity of the nanofiber was recorded in real time to ensure that the output was stable and then, at a specific time, a solid sample of 2,4-DNT (51 mg) was gently placed onto the metal mesh support above the nanofiber array. The emission intensity of the selected nanofiber was then recorded over a period of *ca.* 6 min. Note that a relatively large spot size (full-width-at-half-maximum (FWHM) of *ca.* 0.4 μm) was employed for the focused laser beam during these measurements in order to eliminate any artefacts that might be caused by mechanical drift of the scanning stage within the timeframe of the experiment. Following this, a second confocal emission intensity image and PL spectrum were recorded for the fiber.

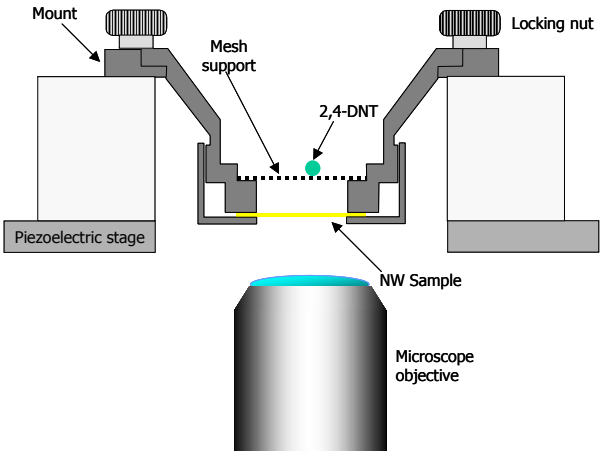

Scheme SI.2 Schematic depiction of the arrangement of the nanofiber sample and of the solid 2,4-DNT material employed during monitoring of single nanofiber emission quenching.

Optical and Morphological Characteristics of PFO Thin Films

Typical intensity-normalized absorption and PL spectra acquired for a PFO solution (5 μg/mL in chloroform), a *ca.* 6.5 nm thick PFO film spun cast onto glass from chloroform solution (0.5 mg/mL, 6000 rpm, 60 s), and the same PFO film following exposure to toluene vapor for 20 min are shown in Figure SI.1. The solution absorption spectrum exhibited an absorption onset at *ca.* 406 nm and a single band at *ca.* 390 nm with a full-width-at-half-maximum (FWHM) of *ca.* 50 nm. The film absorption spectrum exhibited an absorption onset at *ca.* 416 nm and a single band at *ca.* 395 nm with a FWHM of *ca.* 52 nm, assigned to the inhomogeneously broadened $S_0 \rightarrow S_1$ 0–0 transition of amorphous or glassy phase PFO.[1,2] The absorption spectrum of the toluene vapor-treated film was red shifted and slightly broader (main band at *ca.* 395 nm with a FWHM of *ca.* 51 nm) with a shoulder near 401 nm and a pronounced low energy peak at 435 nm characteristic of the $S_0 \rightarrow S_1$ 0–1 and 0–0 transitions of β-phase PFO, respectively.[2,3]

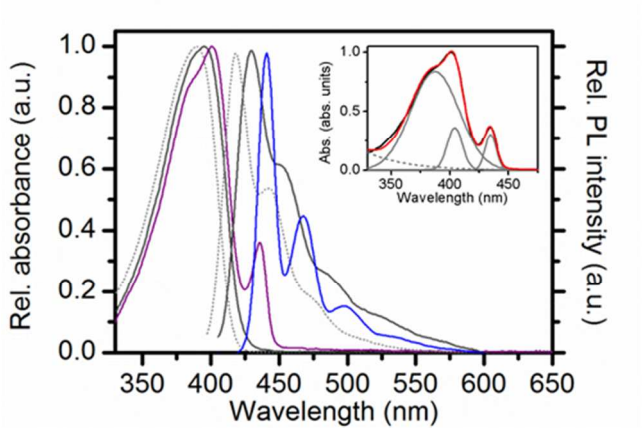

Figure SI.1 Intensity-normalized absorption and emission spectra of a PFO solution (λ_{ex}: 390 nm) (dotted lines), a PFO thin film (λ_{ex}: 395 nm) (grey lines), and the same film following toluene exposure (λ_{ex}: 401 nm) (mauve and blue lines). Inset: Plot of three Gaussian functions (solid grey lines) and a background Gaussian function (dashed grey line) that were fitted to a typical absorption spectrum measured for a toluene vapor-treated film (solid black line). The sum of all four Gaussians is shown (red line).

The fraction of the β-phase material present within the film was estimated by first de-convoluting the absorption spectrum by fitting it with three Gaussian functions using a non-linear least squares algorithm; see Figure SI.1 inset.[4] An additional Gaussian was fit to the data to account for the background signal, mainly due to optical scattering from the film. The amount of β-phase present was taken to be the sum of the areas of the fitted Gaussians centered at 405 nm and 435 nm divided by the total area of all Gaussians (neglecting the background and scattering contributions). An upper limit value for the β-phase fraction of 7 % was determined. According to Chunwaschirasiri *et al.*, the larger oscillator strength of the β-phase in comparison to the other PFO conformers should be considered when estimating β-phase fraction from absorption spectra.[5] Therefore, the fraction of β-phase estimated from absorption spectra in this work was considered to be an upper limit.

The PL spectrum of the PFO solution exhibited a characteristic vibronic progression with peaks centered at 418, 443 and 475 nm arising from the $S_1 \rightarrow S_0$ 0–0 transition of PFO with 0–1 and 0–2 vibronic replicas, respectively.[6] The PL spectrum of the as-spun PFO film exhibited a characteristic vibronic progression with peaks centered at 429, 453 and 484 nm arising from the $S_1 \rightarrow S_0$ 0–0 transition of glassy phase PFO with 0–1 and 0–2 vibronic replicas, respectively.[2] This spectrum was red-shifted with respect to the solution spectrum by *ca.* 10 nm, likely due to an increase in the dielectric constant of the environment around each chromophore as well as increased Förster energy transfer between nearby chromophores in the solid film. The latter effect would favor transfer of energy to, and luminescence from, longer, lower energy polymer segments.[3] By comparison, the PL spectrum of the solvent-treated PFO film exhibited a characteristic vibronic progression with significantly red shifted and narrower peaks centered at 441, 468 and 498 nm indicative of a narrowed distribution of emitting PFO chain segments with

increased effective conjugation. This spectrum was characteristic of the $S_1 \rightarrow S_0$ 0–0 transition of β-phase PFO, with associated 0–1 and 0–2 vibronic replicas, respectively.[2,3]

Overall, the spectroscopic data indicated that a fraction of the glassy phase PFO molecules, with initially random molecular chain conformations, within the toluene vapor-treated films had adopted the more planar (*ca.* 160° torsion angle between neighboring monomers) and extended 2_1 helical molecular conformation of the β-phase during toluene solvent vapor exposure over 20 min; see Scheme SI.3. The emission spectra of solvent treated PFO films were completely dominated by this fraction, due either to Förster-type energy transfer or to singlet exciton migration from the glassy phase to the lower energy β-phase.[1,3,7] In this respect, the β-phase containing PFO films could be regarded as self-doped systems in which a fraction of chains with lower energy gap were intimately dispersed in a host matrix of polymer chains with larger energy gap. The formation of the β-phase within thin films was attributed to the action of mechanical stresses that arose within the films during solvent vapor exposure.[2,8]

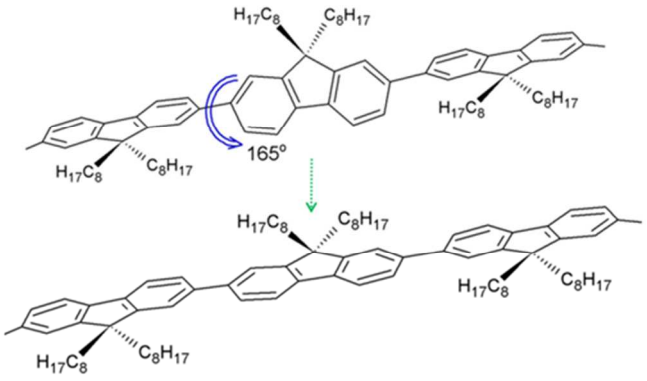

Scheme SI.3 Schematic representation of the PFO molecular structure highlighting differences in monomer arrangements between amorphous phase PFO (top) and β-phase PFO (bottom).

Atomic force microscopy (AFM) images of amorphous phase and β-phase containing PFO thin films on glass substrates were obtained in tapping mode; see Figure SI.2. An average film thickness of *ca.* 6.5 ± 0.3 nm was observed. The films exhibited relatively smooth surface morphologies (RMS surface roughnesses of *ca.* 0.2 ± 0.05 nm) without obvious structural defects. The general agreement in the thickness and roughness values obtained for the amorphous and β-phase films indicated that the external film morphology apparently changed very little following induction of the β-phase molecular conformation.

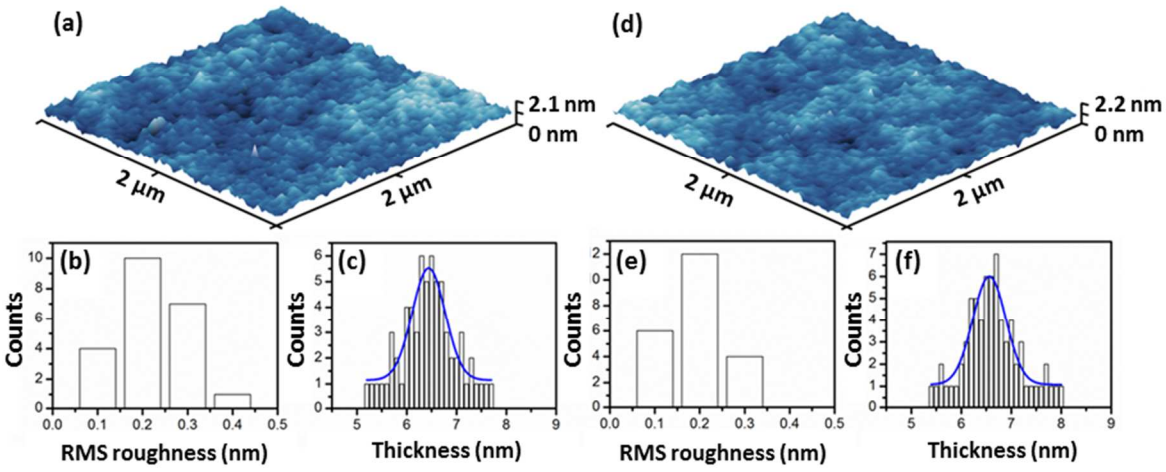

Figure SI.2 Tapping mode atomic force microscopy images of (a) an as-spun PFO thin film, and (d) the same film following toluene vapor exposure. Corresponding RMS roughness and film thickness data for (b) and (c) the as-spun film, and (e) and (f) the vapor-treated film. The solid blue lines shown in (c) and (e) are Gaussian fits to the film thickness data distributions.

Luminescence Response of PFO Thin Films to Vapors of an Electron Deficient Analyte

In order to probe the photoluminescence behavior of PFO thin films in the presence of vapors of an electron deficient analyte, as-spun and toluene solvent-treated films were individually exposed to solid DQ material (that was pre-sealed in cuvettes for 1 hr in advance in order to allow the analyte reach its equilibrium vapor pressure) for specific periods of time prior to measuring PL spectra. Figure SI.3 shows PL spectra acquired for typical, *ca.* 6.5 nm thick, PFO films on glass substrates following exposure to DQ vapors for 0, 10, 30, 60, 120, 180, 300 and

600 s, respectively. For the as-spun film, exposure to DQ resulted in a marked quenching of the amorphous phase PFO emission; see Figure SI.3 (a). The time dependence of the quenching response was determined by monitoring the intensity of the 0–1 emission peak, centered at 459 nm, as a function of exposure time; see Figure SI.3 (b) inset (filled blue squares with solid blue line). A decrease in film emission intensity of 80 % was observed after 10 s, which progressed to 88 % after 60 s.

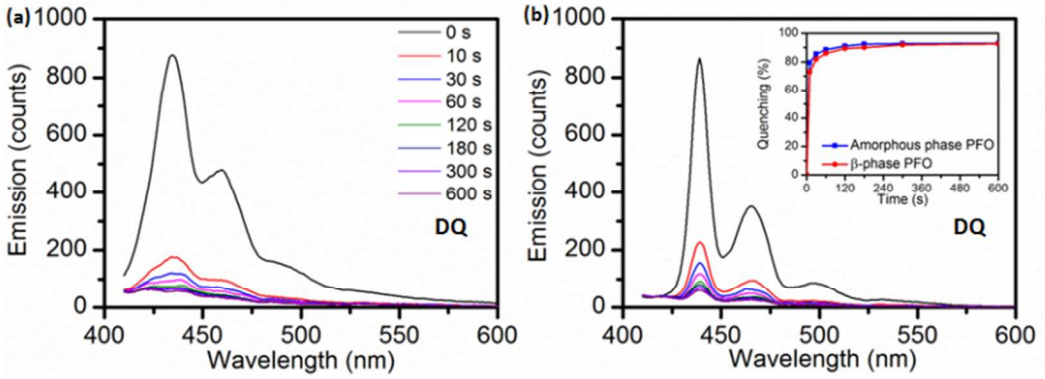

Figure SI.3 (a) Emission spectra (λ_{ex}: 401 nm) recorded for an as-spun PFO thin film upon exposure to duroquinone (DQ) vapor for different times. (b) Emission spectra (λ_{ex}: 401 nm) recorded for a toluene vapor-treated PFO thin film upon subsequent exposure to DQ vapor for different times. Inset: Extent of emission quenching (decay of 0–1 peak intensity) for the as-spun PFO film (blue) and the solvent-treated PFO film (red) as a function of exposure time.

For the toluene-vapor treated PFO film, exposure to DQ resulted in a marked quenching of the β-phase PFO emission; see Figure SI.3 (b). The time dependence of the quenching response was determined by monitoring the intensity of the 0–1 emission peak, centered at 467 nm, as a function of exposure time; see Figure SI.3 (b) inset (filled red squares with solid red line). A decrease in film emission intensity of 73 % was observed after 10 s, which progressed to 86 % after 60 s. Therefore, the quenching behaviors observed for the amorphous phase and the β-phase containing PFO thin films were broadly similar.

The fact that the data of Figure SI.3 indicated that no significant difference in quenching behavior was observed between amorphous phase and β-phase containing thin films following exposure to DQ vapor was unexpected as it was reported by Swager *et al.*[9,10] that the

fluorescence quenching response depends on the porosity of the polymer medium and the electronic properties of the polymer. In this regard, the presence of the β-phase in a PFO film might be expected to offer some advantages as it has been shown that this phase is induced by swelling stress during solvent vapor exposure,[2] and it has been suggested that β-phase chains fold back on themselves to form sheet-like lamellar structures distributed in an amorphous matrix.[11] In this way, β-phase formation could result in the development of voids at the interfaces between the lamellae and the amorphous regions leading to an increase in the free volume. In other words, local porosity might be induced around β-phase clusters facilitating diffusion of analyte molecules within the PFO material. In addition, as mentioned above, only a small fraction of the β-phase will completely dominate the emission characteristics of PFO as a result of ultra-fast migration of excitons (estimated to be < 5 ps)[3] to the lower energy (larger conjugation length) β-phase chain segments. Furthermore, β-phase PFO has been shown to act as an electron trap and to exhibit higher hole mobility,[12,13] making it more likely for an electron deficient molecule to interact with and bind to a β-phase segment. However, the observation that the emission quenching responses of amorphous phase and β-phase containing thin films were very similar during DQ analyte vapor exposure suggested that the presence of a small fraction of the more planar and extended β-phase molecular chain conformation in the solvent treated PFO films provided no emission quenching performance advantage.

Absorption Spectra of the Electron Deficient Analytes

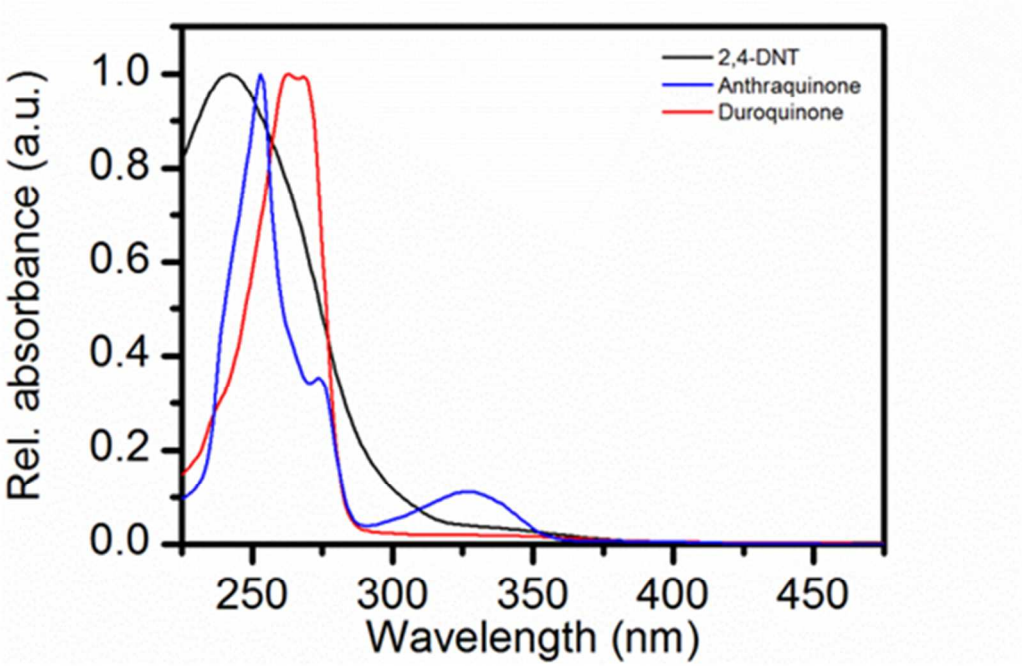

Figure SI.4 Absorption spectra recorded for 2,4-DNT, AQ and DQ dissolved in methanol solutions at a concentration of 50 μM.

Comparative Quenching Responses

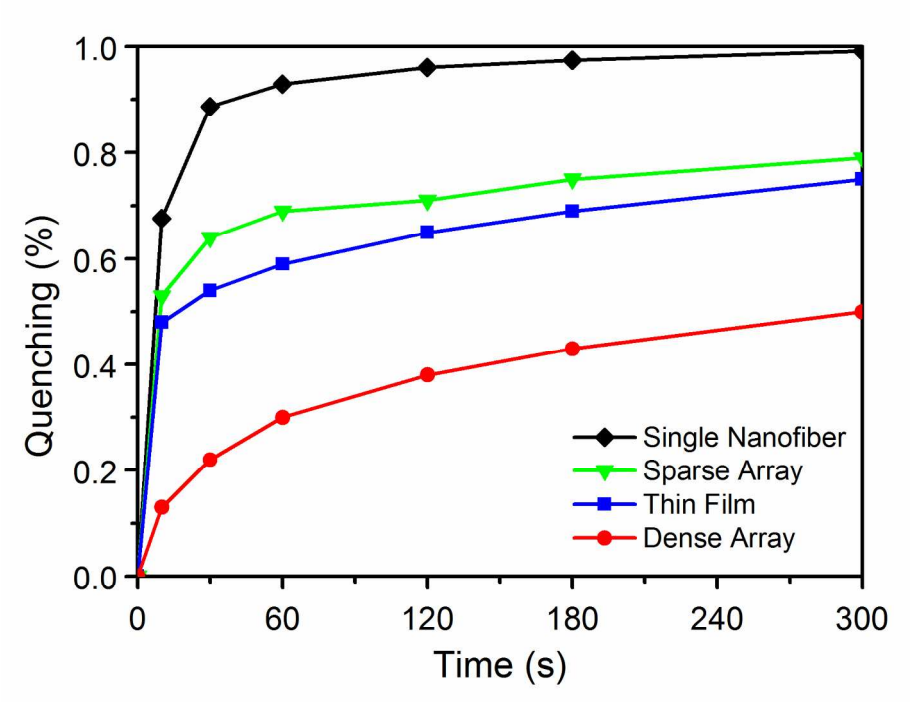

Figure SI.5 Extent of PL quenching (decay of 0–1 peak intensity) for single nanofiber, nanofiber array and thin films samples as a function of exposure to 2,4-DNT, and AQ, respectively.

Energy Level Alignments and Other Physical Parameters in the PFO / Analyte System

Polymers & analytes	GPC Mn (PDI)	Abs/PL λ_{max} (eV)	E_g (eV)	E_A (eV)	IP (eV)	E_{red} (V *vs.* SCE)	Vapor pressure (mm Hg at 25 ^{o}C)
PFO (amorphous)	100,000	395/429 (film)	3.7	2.1	5.8		
PFO (β-phase)		401/441 (film)	3.6	2.2	5.8		
2,4-DNT		407/444 (NF mat)				- 1.0	1.47×10^{-4}
AQ						- 0.9	1.16×10^{-7}
DQ						- 0.8	2.88×10^{-3}

Table SI.1. Relevant physical properties of polymer and analytes.[12,14-17]

A schematic representation of the energetically favorable nature of this process of oxidative electron transfer between glassy phase (and β-phase) PFO and 2,4-DNT, AQ and DQ is shown in Scheme SI.4. In this scheme, the energies of the lowest unoccupied molecular orbitals (LUMOs) and highest occupied molecular orbitals (HOMOs) of PFO and analytes are presented.

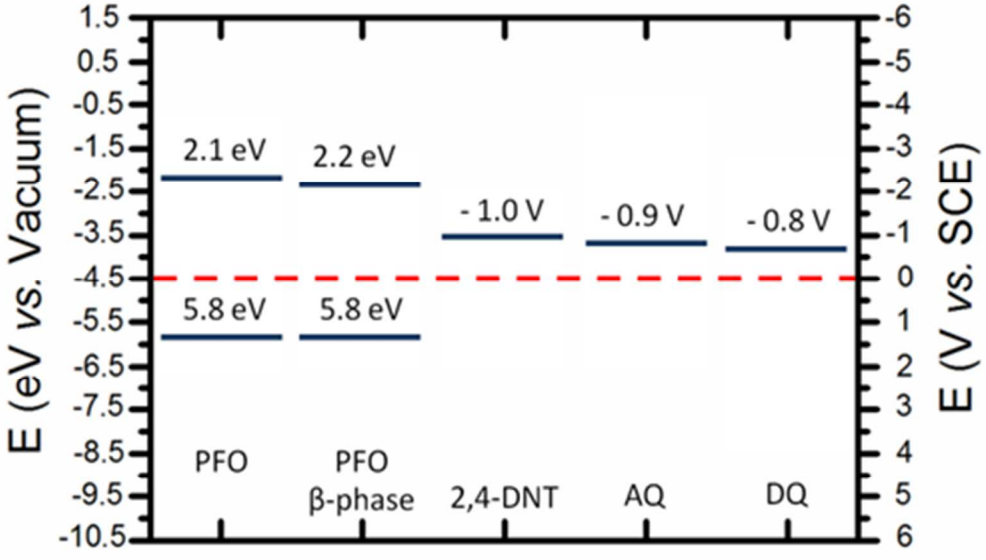

Scheme SI.4 Simplified energy level diagram showing the LUMO (π*) and HOMO (π) levels of amorphous and β-phase PFO, and the LUMO levels of 2,4-DNT, AQ and DQ, respectively.

Polymers and analytes	$\Delta\delta_d$ $[MJ/m^3]^{1/2}$	$\Delta\delta_p$ $[MJ/m^3]^{1/2}$	$\Delta\delta_h$ $[MJ/m^3]^{1/2}$
PFO	20.86	0.23	0
2,4-DNT	20.55	11.59	4.79
AQ	42.7	0	4.41
DQ	24.55	0	3.89

Table SI.2. Estimated values for solubility parameters of the PFO polymer and the three analytes studied. δ_d, δ_p and δ_h, are the solubility parameters associated with dispersion forces, polar forces and hydrogen bonding, respectively.[18]

Polymers and analytes	$\Delta\delta_d$ $[MJ/m^3]^{1/2}$	$\Delta\delta_p$ $[MJ/m^3]^{1/2}$	$\Delta\delta_h$ $[MJ/m^3]^{1/2}$	$\Delta\delta$ $[MJ/m^3]^{1/2}$
2,4-DNT/PFO	-0.3	11.36	4.79	12.33
AQ/PFO	21.84	-0.23	4.41	22.28
DQ/PFO	3.69	-0.23	3.89	5.37

Table SI.3. Estimated difference values for solubility parameters for the three polymer/analyte pairs studied. $\Delta\delta_d$, $\Delta\delta_p$ and $\Delta\delta_h$ are the differences in the solubility parameter values associated with dispersion forces, polar forces and hydrogen bonding, respectively, between the PFO polymer and each analyte. Also, $\Delta\delta = [(\Delta\delta_d)^2 + (\Delta\delta_p)^2 + (\Delta\delta_h)^2]^{1/2}$.[18]

References

(1) Ariu, M.; Lidzey, D. G.; Sims, M.; Cadby, A. J.; Lane, P. A.; Bradley, D. D. C. *J. Phys. Condens. Matter* **2002**, *14*, 9975.

(2) Grell, M.; Bradley, D. D. C.; Ungar, G.; Hill, J.; Whitehead, K. S. *Macromolecules* **1999**, *32*, 5810-5817.

(3) Ariu, M.; Sims, M.; Rahn, M. D.; Hill, J.; Fox, A. M.; Lidzey, D. G.; Oda, M.; Cabanillas-Gonzalez, J.; Bradley, D. D. C. *Phys. Rev. B* **2003**, *67*, 195333.

(4) Worsfold, O.; Hill, J.; Heriot, S. Y.; Fox, A. M.; Bradley, D. D. C.; Richardson, T. H. *Mater. Sci. Eng., C* **2003**, *23*, 541-544.

(5) Chunwaschirasiri, W.; Tanto, B.; Huber, D.; Winokur, M. *Phys. Rev. Lett.* **2005**, *94*, 107402.

(6) Teetsov, J.; Anne Fox, M. *J. Mater. Chem.* **1999**, *9*, 2117-2122.

(7) Khan, A.; Sreearunothai, P.; Herz, L.; Banach, M.; Köhler, A. *Phys. Rev. B* **2004**, *69*, 085201.

(8) Chen, S. H.; Su, A. C.; Chen, S. A. *J. Phys. Chem. B* **2005**, *109*, 10067-10072.

(9) Thomas, S. W.; Joly, G. D.; Swager, T. M. *Chem. Rev.* **2007**, *107*, 1339-1386.

(10) Yang, J. S.; Swager, T. M. *J. Am. Chem. Soc.* **1998**, *120*, 11864-11873.

(11) Kitts, C. C.; Vanden Bout, D. A. *Polymer* **2007**, *48*, 2322-2330.

(12) Lu, H. H.; Liu, C. Y.; Chang, C. H.; Chen, S. A. *Adv. Mater.* **2007**, *19*, 2574-2579.

(13) Prins, P.; Grozema, F. C.; Nehls, B. S.; Farrell, T.; Scherf, U.; Siebbeles, L. D. A. *Phys. Rev. B* **2006**, *74*, 113203.

(14) Chen, R.-F.; Zhu, R.; Fan, Q.-L.; Huang, W. *Org. Lett.* **2008**, *10*, 2913-2916.

(15) Gong, X.; Moses, D.; Heeger, A. J.; Xiao, S. *Synth. Met.* **2004**, *141*, 17-20.

(16) Liao, J.-L.; Chen, X.; Liu, C.-Y.; Chen, S.-A.; Su, C.-H.; Sut, A.-C. *J. Phys. Chem. B* **2007**, *111*, 10379-10385.

(17) Ma, W. L.; Iyer, P. K.; Gong, X.; Liu, B.; Moses, D.; Bazan, G. C.; Heeger, A. J. *Adv. Mater.* **2005**, *17*, 274-277.

(18) van Krevelen, D. W.; te Nijenhuis, K. *Properties of Polymers*, 4th ed.; Elsevier: Amsterdam, 2009.